MULTI BLOCK NAVIER STOKES SOLUTIONS OF LOW ASPECT RATIO RECTANGULAR FLAT WINGS IN COMPRESSIBLE FLOW

Gökhan Durmuş, Mehmet Şerif Kavsaoğlu
Middle East Technical University, 06531 Ankara, Turkey

Keywords: *vortex flows, flow separation, parallel process*

Abstract

Two block parallel Navier Stokes solutions of an aspect ratio 1.0 flat plate with sharp edges are obtained at different Mach numbers and angles of attack. Reynolds numbers are of the order of $2.0*10^5$-$3.0*10^5$. The flow field is dominated by vortices and separated flows. In two blocks total of 700,000 grid points are used. In the normal direction the initial spacing from the surface is taken as 0.0001 of the chord length. The flow is assumed to be laminar for the first 75 % of the chord and turbulent for the rest. Baldwin Lomax turbulence model is used in the turbulent regions. Due to the fine features of the grids the convergence of the solutions are slow but steady. Strong side edge vortices are predicted easily. Prediction of the leading edge separation bubble is found to be a slowly converging phenomenon.

1 Introduction

Low aspect ratio rectangular flat wings are in general used in missiles. Some of the missiles which are donated with these wings fly and maneuver at high angles of attacks. General description of the flow field is shown in Figure 1. Flow separates at the sharp leading edge and forms the leading edge bubble. There are also two side edge vortices which are similar to the leading edge vortices of Delta wings. In general missile aerodynamics and high angle of attack aerodynamics are dominated with vortical and separated flows. Various publications by AGARD provide a large selection of research results in this field [1-6]. Low aspect ratio rectangular flat wings were studied much less when compared to the Delta wings of the similar nature. Stahl [7] summarized some of the early research works. Winter [8] obtained pressure distributions on the suction side and force and moment measurements of various low aspect ratio rectangular flat wings at incompressible speeds. At von Karman Institute similar experiments were performed in a transonic wind tunnel for higher speeds [9, 10].

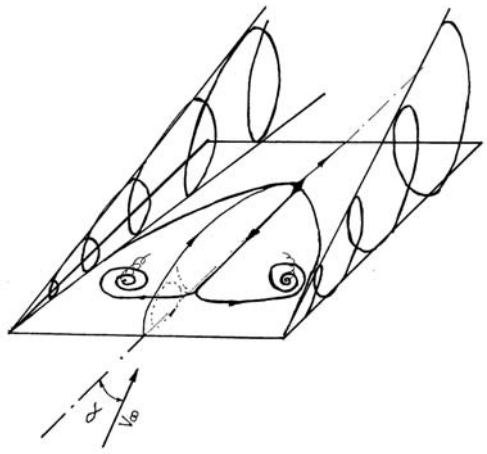

Fig. 1. General description of the flow field [10].

In the present study the experiments of van Westerhoven *et. al*[9]. and Kavsaoğlu[10] are taken as test cases for comparison of the results. The geometry of the flat wing is shown in Fig. 5. In a previous study, single block Navier Stokes analysis of these flowfields was obtained[11]. Single block structured grids face the grid skewness problem around the sharp corners which may reduce the accuracy of the solutions. A sample single block grid around a sharp corner is seen in Fig. 6. In the present study

multi block approach is tested by using a zonal, parallel, Navier Stokes solver[12].

2 Navier Stokes Equations

The thin layer Navier Stokes Equations written in curvilinear coordinates in strong conservation form are given in equation 1.

$$Q_\tau + E_\xi + F_\eta + G_\zeta = \frac{1}{Re}\left(S_{1_\xi} + S_{2_\eta} + S_{3_\zeta}\right) \qquad (1)$$

Here Q is the dependent variable vector, $Q = J^{-1}[\rho, \rho u, \rho v, \rho w, e]^T$, J is the transformation Jacobian, E, F, G are the inviscid flux vectors, S_1, S_2, S_3 are the thin layer viscous flux vectors in each curvilinear direction, and Re is the Reynolds number.

3 Solution Algorithm

A parallel, multi block, time marching Navier Stokes solver is used [12]. The thin layer Navier Stokes equations are discretized by using the Beam and Warming [13] finite difference implicit algorithm. The matrix solution is carried out using a diagonally dominant LU-ADI factorization algorithm [14]. Baldwin Lomax [15] model is used for turbulence modeling.

Multi block technique is used to reduce geometrically complex regions into several smaller, more manageable regions, called as blocks. There are two options available for data transfer between the blocks [12]. In the first option, cell to cell matching between block boundaries is maintained. This method eliminates complex interpolations between the blocks. In the second option, cell to cell matching on the block boundaries is ignored. This method offers some flexibility such as using H type grid in one block and O type grid in the adjacent block. The different blocks are solved as parallel processes. The Message Passing Interface (MPI) [16] library was used for communication between the processes.

4 Experimental Data For Comparison

The test cases are selected from the experimental data at the von Karman Institute (VKI) [9, 10]. Test models are low aspect ratio, rectangular flat plates with small thickness and sharp edges. Model aspect ratios (AR) are 0.5, 0.67, 1.0 and 1.5. For AR=1.0, the low speed model dimensions are 100mm*100mm*5mm and the high speed force model dimensions are 80mm*80mm*2mm. The high speed pressure model dimensions are 100m*100mm. Front and side edges of the models are sharp. The top surfaces of the models are not deflected at the edges and connect to the lower surfaces with 15° angle. In Figure 2, the top and side view drawings of the model used for high speed oil flow measurements are shown.

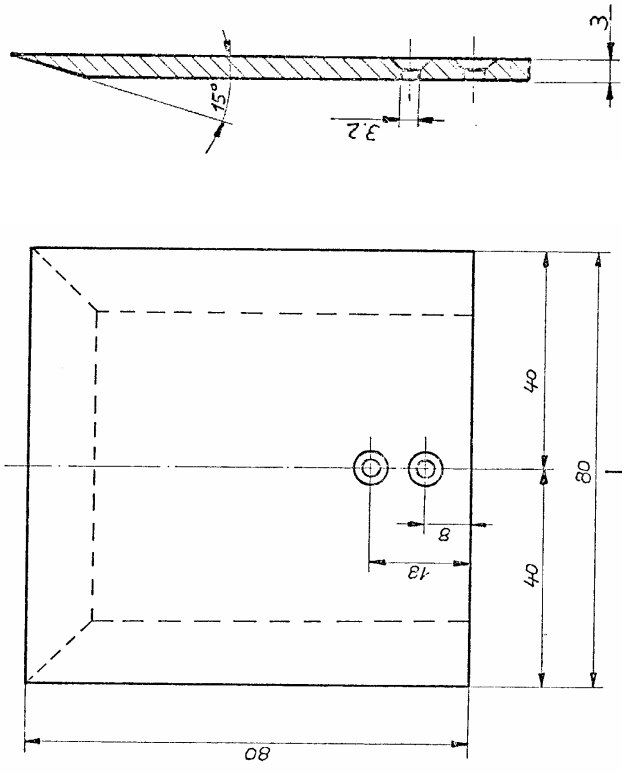

Fig. 2. Model used for compressible oil flow tests [10].

The experiments include surface oil flow measurements, force and moment measurements

and surface pressure distribution measurements. Low speed tests were carried out in the VKI low speed, open circuit wind tunnel of the suction type, designated L-2A. This tunnel has a 0.3 m diameter circular test section. Maximum tunnel velocity is 40 m/sec and the Reynolds number based on the model chord length is about $2*10^5$. At low speeds, oil flow visualizations were performed at different angles of attack varying from 0° to 40°. High speed subsonic tests were carried out in the VKI S-1 wind tunnel. This is a closed circuit transonic / supersonic wind tunnel with 0.4 m * 0.4 m test section. Subsonic tests are performed in the transonic test section with slotted horizontal walls. High speed tests include surface pressure distribution measurements, force and moment measurements and a few oil flow measurements. Mach number range was 0.4-0.9. Reynolds numbers varied between $1.63*10^5$ and $2.62*10^5$.

For the present computational study an aspect ratio 1.0 flat plate with zero thickness is considered as the test model. The computational test matrix is given in Table 1.

CASE	M_∞	Re_∞	α (deg)
P1	0.54	$3.0*10^5$	7.5
P2	0.55	$3.0*10^5$	13.5
P3	0.87	$3.0*10^5$	7.5
P4	0.85	$3.0*10^5$	13.5
S1	0.42	$1.65*10^5$	5
S2	0.42	$1.65*10^5$	15

Table 1. Computational test matrix.

The cases P1-P4 are intended for pressure comparisons and the cases S1, S2 are intended for surface streamline comparisons.

5 Grid

The flow field is symmetric with respect to the *xz* plane. Therefore, only the half of the flat plate is considered for grid generation. The computational domain is divided into two zones. The first zone is above the flat plate and extends in the range of $-3.0 \le x/c \le 4.0$, $0.0 \le y/c \le 3.5$ and $0.0 \le z/c < 3.0$. The second zone is below the flat plate and extends in the range of $-3.0 \le x/c \le 4.0$, $0.0 \le y/c \le 3.5$ and $-3.0 < z/c \le 0.0$. The flat plate lies in the z=0.0 plane and it extends in the range $0.0 \le x/c \le 1.0$ and $0.0 \le y/c \le 0.5$. Two grids are produced, one for the first zone (top) and the other one for the second zone (bottom). They are named as BLOCK1 and BLOCK2. These grid blocks are seen in Figure 3.

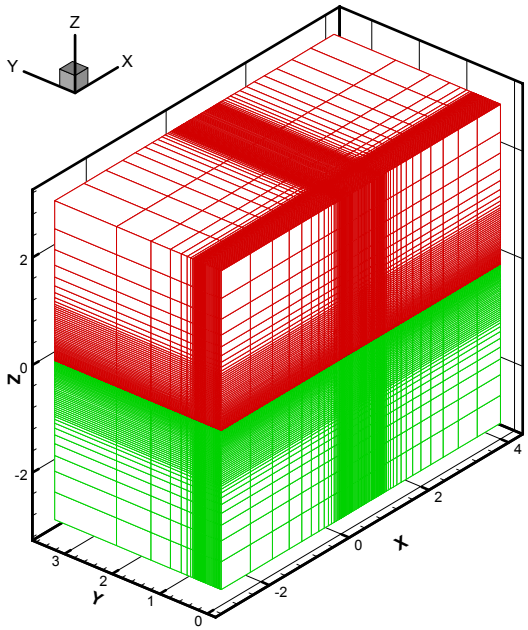

Fig. 3. Overall view of the grid blocks, BLOCK1 and BLOCK2.

In Figure 4, the grid details around the flat plate at the symmetry plane (y/c=0.0) are shown. In Figure 5, the top view of the grid at z/c=0.0 plane is shown. In this figure the red colored locations belong to the flat plate where the no slip boundary condition is applied. At the green colored locations matched surface boundary conditions are applied for data transfer between lower and upper block solutions. For the top grid (BLOCK1), the grid dimensions are JMAX*KMAX*LMAX = 100*50*70 points in ξ, η, ζ directions. On the flat plate surface

there are 61 points in ξ direction and 35 points in η direction. The first grid distance in ζ direction from the flat plate surface is $\Delta z/c = 0.0001$. A three dimensional hyperbolic grid generation code [17] is used to produce this grid. In ζ direction, four different stretching ratios are used in four different regions to obtain desired grid densities. These regions are $0.0 \le z/c \le 0.1$, $0.1 \le z/c \le 0.5$, $0.5 \le z/c \le 1.0$, and $z/c > 1.0$. The total number of points up to z/c = 1.0 is 60. The bottom grid (BLOCK2) is the symmetric of BLOCK1 with respect to the z/c = 0.0 plane and has the same dimensions. Thus in two blocks total of 700,000 grid points were produced.

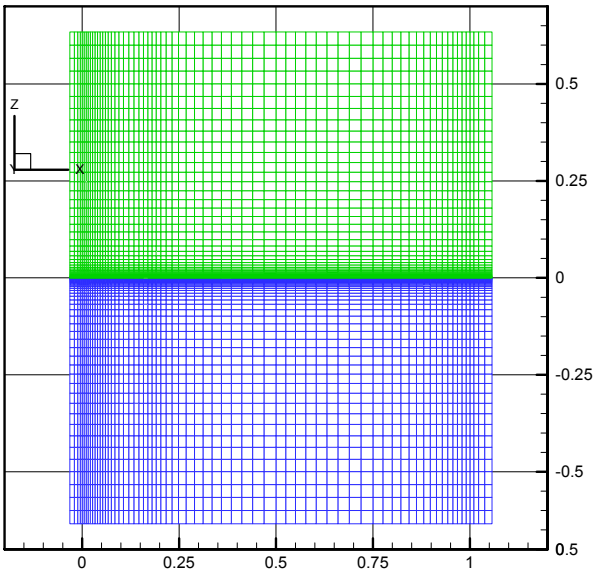

Fig. 4. Symmetry plane (y/c=0) view of the grid around the flat plate.

6 Boundary Conditions

The boundary conditions are applied as follows. At the front (x/c=-0.3) and bottom surfaces ($z/c \simeq$ -0.3) the free stream conditions are applied. At the symmetry plane (y/c = 0.0) the symmetry conditions are applied. At the top ($z/c \simeq 0.3$), back (x/c=-0.3) and side (y/c = 3.5) extrapolation type boundary conditions are applied. At the upper and lower flat plate surfaces the no slip conditions are applied (z/c=0.0). At the interface between upper and lower blocks, excluding the flat plate, the matched surface boundary conditions are applied [12].

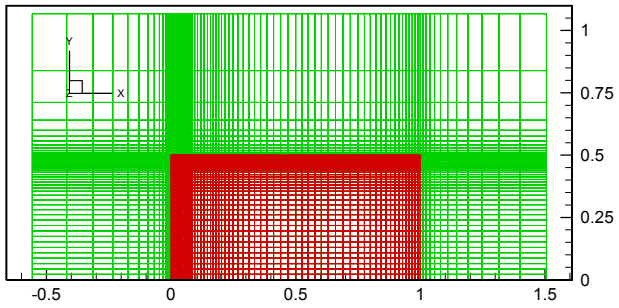

Fig. 5 Top view of the grid at z/c=0.0 plane.

7 Computational Details

Computations are performed on 8 dual Pentium-III 700Mhz processor workstations which serve as the parallel computing environment for the Department of Aerospace Engineering, Middle East Technical University. Each workstation has 512 MB of RAM. Each test case is run on a workstation as two block parallel processes. A two block parallel solution with 2*350,000 grid points requires 2*82 MB of RAM. Approximately 412 minutes of CPU time is needed per 1000 iterations.

8 Results

In figure 6 a typical convergence history is shown. This figure shows the convergence of the L2 norm of the residual for the first 30,000 iterations for the case: P1 described in Table 1. The jump at 20,000 iterations for the lower block (BLOCK2) is due to a correction made on the matched surface boundary conditions of this block. For the first 21,000 iterations the Baldwin Lomax turbulence model was applied all over the flat plate surface and the results did

not show flow separation at the center-plane (y/c=0.0). This was not in agreement with the experimental data. Although the solution was not converged sufficiently, after the first 21,000 iterations, it was decided to assume laminar flow up to x/c=0.75 and turbulent flow for $x/c > 0.75$. This was the reason for the small increase, particularly observable, in the upper block (BLOCK1) convergence history. For the first 21000 iterations the CFL number was taken as 10.0 and after this it was reduced to 5.0.

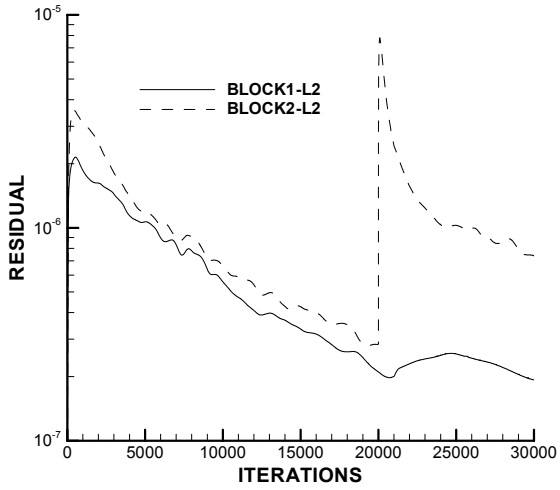

Fig. 6 Convergence history of the case: P1.

The convergence is steady but very slow. For a comparison, in Fig. 7 a typical convergence history for a similar case obtained in a previous study [11] is shown. A similar flow solver was used, and it can be seen that, L2 norm of the residual was reduced more than 3 orders of magnitude in 5000 iterations with CFL=1.0. For this case a single block grid with 107,457 points was used [11]. This grid size is quite small when compared to the present grid (total of 700,000 points in two blocks). Another difference is the initial grid spacing in ζ direction from the surface. For the present case $\Delta z/c$ = 0.0001, which is much smaller when compared to the $\Delta z/c$ = 0.0018 of Ref. [11]. These may be the reasons for slower convergence of the present cases.

The following results are obtained after the first 30,000 iterations of the test cases described in Table. 1. Therefore they are not fully converged results. Computations are continuing and more accurate results are expected to be obtained at the time of the ICAS 2002 conference.

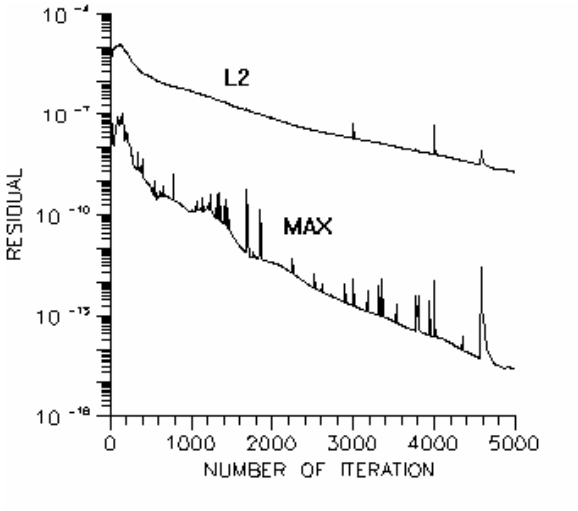

Fig. 7 A typical convergence history with a single block grid with 107,457 points, α = 7.5°, Mach = 0.54, $Re = 3*10^5$, CFL=1.0 [11].

In Figures 8 and 9, the experimentally obtained surface streamlines by using the oil flow method are shown [10]. These data were obtained in the low speed tunnel for α = 15°. In Fig. 10, the computationally obtained streamlines are shown for the same angle of attack at Mach = 0.42. The formation of the side edge vortices are predicted well. However, the large separation bubble, which covers the mid part of the top surface, is not there. It can be seen that, the formation of this bubble has started from the leading edge, near the corner. The size of the bubble is expected to grow by the increasing number of iterations. Since the side edge vortices are predicted well and the size of the leading edge bubble is not predicted, the pressures around the side edges will also be expected to be predicted better than the centerline pressures.

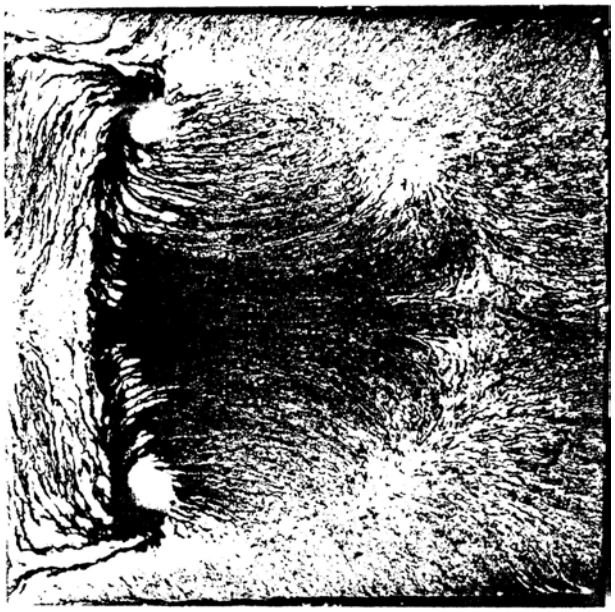

Fig. 8 Experimentally obtained top surface streamlines α=15°, Mach≅0.1, Re=2.0*10^5 [10]. The flow is from left to right.

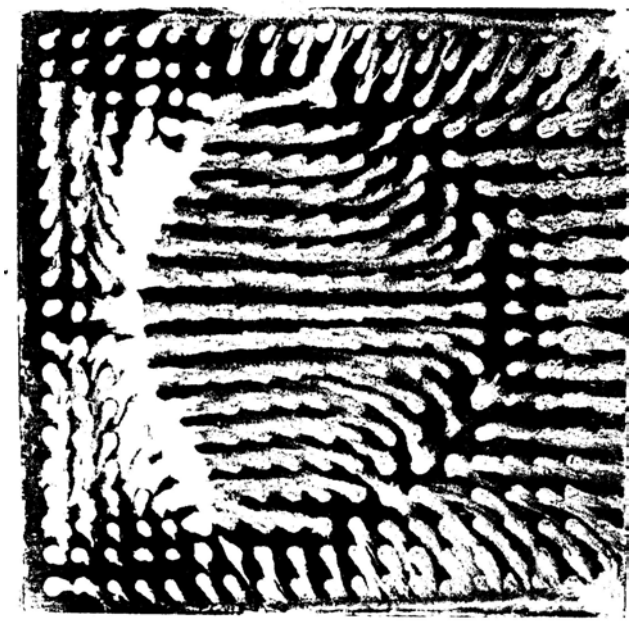

Fig. 9 Experimentally obtained top surface streamlines α=15°, Mach≅0.1, Re=2.0*10^5 [10]. The flow is from left to right.

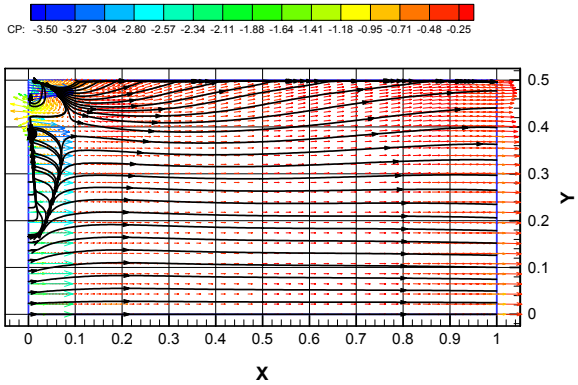

Fig. 10 Computationally obtained top surface streamlines. CASE: S2, α=15°, Mach = 0.42, Re = 1.65*10^5. Symmetric with respect to y/c=0.0.

In Fig. 11, the computed velocity vectors around the side edge, at x/c = 0.5, are shown. This figure clearly shows the side edge vortex on the top surface.

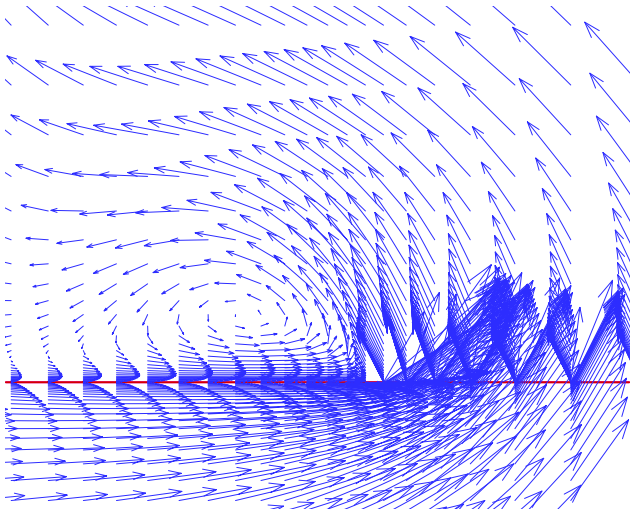

Fig. 11 Computed velocity vectors near the flat plate edge. CASE: S2, α=15°, Mach = 0.42, Re = 1.65*10^5, x/c=0.5.

In Figures 12 through 19 the computed and experimentally obtained surface pressures are compared. As explained before, due to better prediction of the side edge vortices, the side edge pressures agree better with the experimental data. On the other hand, due to

insufficient prediction of the size of the leading edge bubble the computed centerline pressures agree less with the experiment. This can be seen by comparison of the centerline pressures for CASE's P1 and P3 in Figures 16 and 18. The better prediction of the pressures along the side edge can also be observed from Figures 17 and 19 for cases P1 and P3.

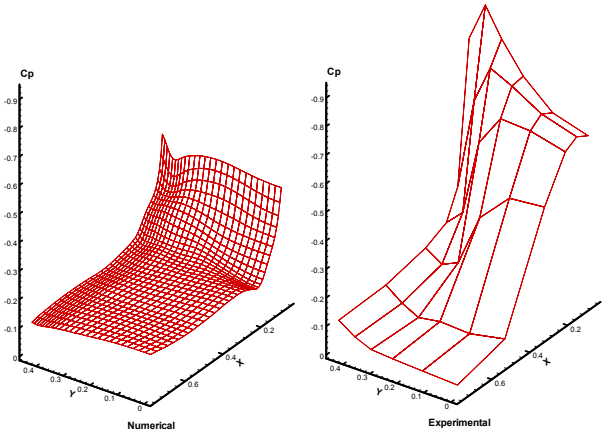

Fig. 12 Comparison of computational and experimental [9] surface pressures. CASE: P1, α=7.5°, Mach = 0.54, *Re* = 3.0*10^5.

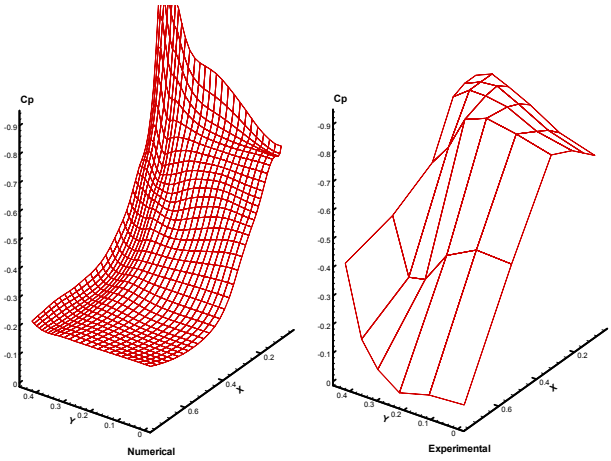

Fig. 13 Comparison of computational and experimental [9] surface pressures. CASE: P2, α=13.5°, Mach = 0.55, *Re* = 3.0*10^5.

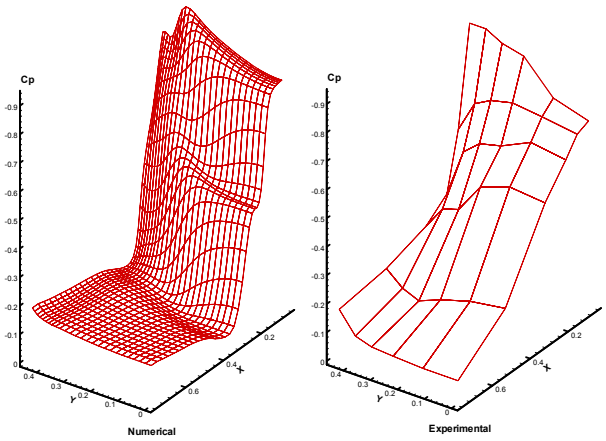

Fig. 14 Comparison of computational and experimental [9] surface pressures. CASE: P3, α=7.5°, Mach = 0.87, *Re* = 3.0*10^5.

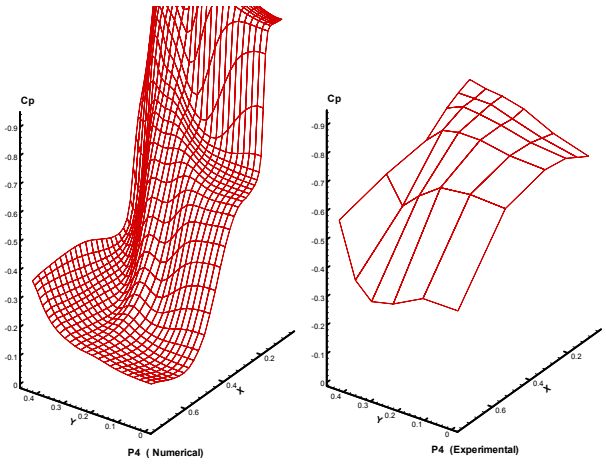

Fig. 15 Comparison of computational and experimental [9] surface pressures. CASE: P4, α=13.5°, Mach = 0.85, *Re* = 3.0*10^5.

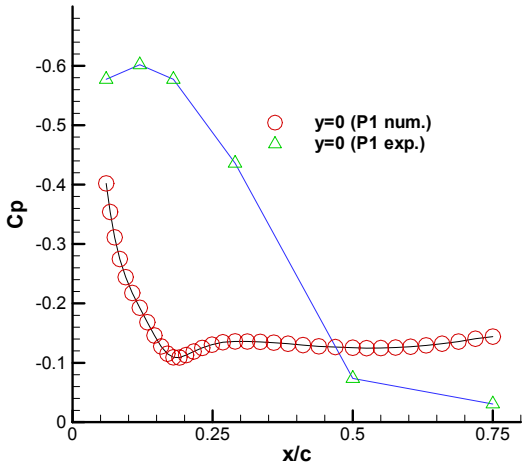

Fig. 16 Comparison of computational and experimental [9] surface pressures along the centerline, y/c=0. CASE: P1, α=7.5°, Mach = 0.54, Re = 3.0*10^5.

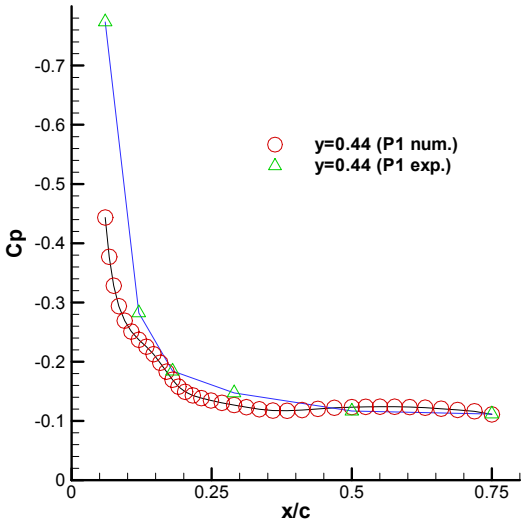

Fig. 17 Comparison of computational and experimental [9] surface pressures near the flat plate side edge, y/c=0.44. CASE: P1, α=7.5°, Mach = 0.54, Re = 3.0*10^5.

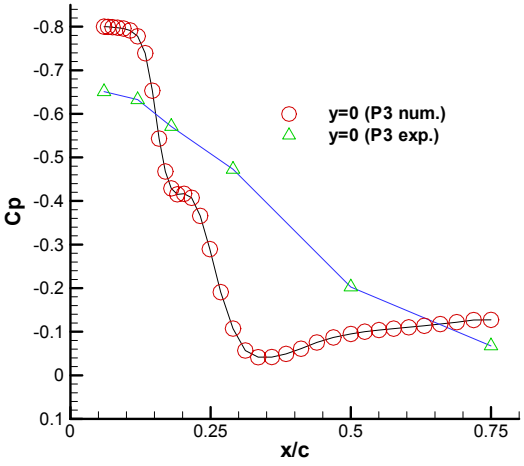

Fig. 18 Comparison of computational and experimental [9] surface pressures along the centerline, y/c=0. CASE: P3, α=7.5°, Mach = 0.87, Re = 3.0*10^5.

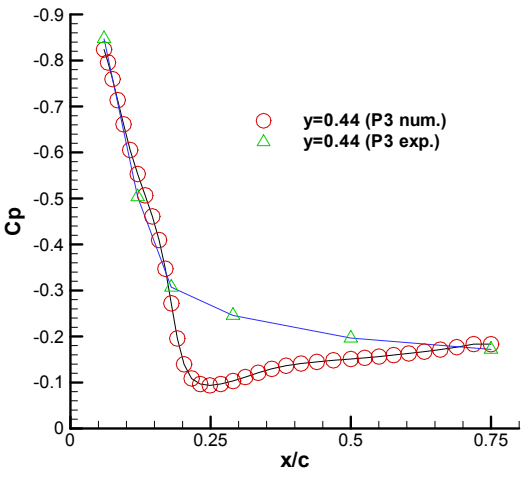

Fig. 19 Comparison of computational and experimental [9] surface pressures near the flat plate side edge, y/c=0.44. CASE: P3, α=7.5°, Mach = 0.87, Re = 3.0*10^5.

In Fig. 20 the computed normal force coefficients are compared with the experimental data for Mach=0.54. Normal force is obtained by the integration of surface pressures from the top and bottom surfaces. Before reaching a conclusion, more normal force predictions need to be performed at different Mach numbers and angles of attack using better converged solutions.

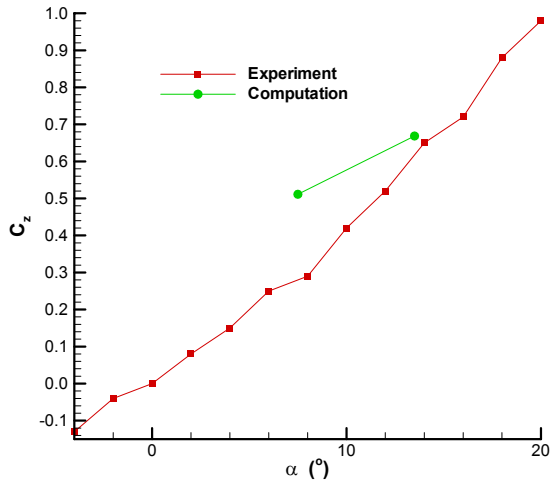

Fig. 20 Comparison of computational and experimental [10] normal force coefficients, Mach = 0.54, $Re = 2.0*10^5$. Computational data from CASE's: P1 and P2.

9 Conclusions

Parallel Navier Stokes solutions of an aspect ratio 1.0 flat plate are obtained at different Mach numbers and angles of attack. Reynolds number was of the order of $2.0*10^5$-$3.0*10^5$. The flow is dominated by with the vortices and flow separation. Due to the low Reynolds numbers, it is assumed to be laminar for the first 75 % of the chord from the leading edge and turbulent for the rest. Two grid blocks with total of 700,000 points are used. The initial grid spacing from the surface in the normal direction is $\Delta z / c = 0.0001$. When the grid is finer, it is expected that the solution converges slower but the results will be more accurate. The results presented here were obtained after the first 30,000 iterations of the different cases. Only about one order of magnitude convergence was achieved after the first 30,000 iterations. The side edge vortices and pressures of the top surface were predicted well. On the other hand, the prediction of the size of the leading edge bubble was insufficient which resulted in the less accurate prediction of the centerline pressures. It is expected that by the growing number of iterations a more converged solution will be obtained and the leading edge separation bubble will also be predicted better.

References

[1] AGARD CP-247, *High Angle of Attack Aerodynamics,* 1979.

[2] AGARD LS-98, *Missile Aerodynamics*, 1979.

[3] AGARD LS-121, *High Angle of Attack Aerodynamics*, 1982.

[4] AGARD CP-494, *Vortex Flow Aerodynamics*, 1991.

[5] AGARD CP-497, *Maneuvering Aerodynamics*, 1991.

[6] AGARD R-776, *Special Course on Aircraft Dynamics at High Angles of Attack: Experiments and Modelling*, 1992.

[7] Stahl W. H., Aerodynamics of Low Aspect Ratio Wings, in AGARD LS-98, *Missile Aerodynamics*, 1979.

[8] Winter H., Strömungsvorgange an Platten und profilierten Körpern bei kleinen Spannweiten. *Forsch. Ing. -Wes.,* Vol. 6, 1935, pp. 40-50, 67-71. Also: Flow Phenomena on Plates and Airfoils of Short Span, *NACA Rep. 798*, 1937.

[9] van Westerhoven P., Wedemeyer E., Wendt J. F., Low Aspect Ratio Rectangular Wings at High Incidences, Paper presented at the *AGARD Symposium on Missile Aerodynamics*, Trondheim, Norway, September 20-22, 1982.

[10] Kavsaoğlu M. Ş, Flow Around Low Aspect Ratio Rectangular Flat Plates Including Compressibility, von Karman Institute For Fluid Dynamics, VKI-PR 1982-15, June 1982.

[11] Laçin F., Kavsaoğlu M., Navier Stokes Analysis of Low Aspect Ratio Rectangular Flat Wings in Compressible Flow, ICAS-94-10.3.3, *19th Congress of the International Council of the Aeronautical Sciences and AIAA Aircraft Systems Conference*, September 18-23, Anaheim, CA, U.S.A.,

[12] Şen T. S., Development of a Three Dimensional Multiblock Parallel Navier Stokes Solver, PhD Thesis, Middle East Technical University, Department of Aeronautical Engineering, November 2001.

[13] Beam, R. W., and Warming, R. F., "An Implicit Finite Difference Algorithm for Hypersonic Systems in Conservation Form, *Journal of Computaional Physics*, Vol. 23, 1976, pp 87-110.

[14] Fujii, K., "Practical Applications of New LU-ADI Scheme for the Three Dimensional Navier-Stokes Computation of Transonic Viscous Flows," *AIAA 24th Aerospace Sciences Meeting*, Reno, Nevada, January, 1986.

[15] Baldwin, B. S., Lomax, H., "Thin Layer Approximation and Algebraic Model for Separated Turbulent Flows," *AIAA 16th Aerospace Meeting*, Huntsville, Alabama, January, 1978.

[16] MPI-2: Extensions to the Message Passing Interface, *Message Passing Interface Forum*, University of Tennessee, Knoxville, Tennessee, July 18, 1997.

[17] Durmuş, G., Three Dimensional Hyperbolic Grid Generation, MS Thesis, Middle East Technical University, Department of Aeronautical Engineering, September 1998.